Conference Proceedings

EuroSun 2016
Palma de Mallorca (Spain), 11 - 14 October 2016

Pressure drop in parallel flow flat-plate PV/T collectors

Esteban Iglesias Manríquez[1,2,3], Laetitia Brottier[1,4] and Rachid Bennacer[4]

[1] DualSun, Marseille (France)

[2] École CentraleSupélec, Paris (France)

[3] Department of Electrical Engineering, Universidad de Chile, Santiago (Chile)

[4]LMT, ENS Cachan, CNRS, Université Paris Saclay, Cachan (France)

Abstract

Pressure drop is known to be an important factor for the efficacy of thermosiphon systems. Accordingly, in this paper a flat-plate PV/T solar collector is studied to predict the pressure drop over it. First, a numerical model of the collector is presented and fluid dynamic concepts are introduced. This is done in order to determine an expression of pressure drop for a given water flow rate over both the collector's channels and manifolds. Then, an algorithm is presented to predict the pressure drop over the whole collector. The effect of the manifold size on the induced pressure drop is investigated. Finally, three flat-plate solar collectors with different manifold dimensions were used as a test case in which the model was validated within 3-8% in terms of normalized root-mean-square deviation. For the case of flat-plate PV/T solar collectors to be used in thermosiphon water systems, this model can be used to investigate trade-offs between fabrication choices and the thermosiphon performance.

Keywords: *Pressure drop, PV/T collector, solar energy, heat exchanger, thermosiphon, DualSun module*

1. Introduction

A solar photovoltaic-thermal (PV/T) collector is a combination of a solar photovoltaic panel (PV) and solar thermal (T) collector which simultaneously convert solar energy into electricity and heat in one integrated system. The photovoltaic cells are in contact with a thermal collector. When the system is operating, the energy from the sun is converted to electricity by the photovoltaic cells on the front side of the panel while a coolant fluid removes heat from the cells on the back side of the panel, generating a double benefit: (1) the collected heat can be used in domestic hot water systems and (2) the cooling of the photovoltaic cells increases the total electricity output as the efficiency of the photovoltaic cells decrease as a function of temperature (Wysocki and Rappaport, 1960).

Fig. 1: A DualSun module being installed in a thermosiphon water system testbed in Marseille, France.

doi:10.18086/eurosun.2016.08.09 Available at http://proceedings.ises.org

Nomenclature:

A	cross-sectional area, m^2
D	diameter, m
f	Darcy friction factor, $-$
g	gravitational constant = 9.81 $\mathrm{m/s^2}$
H	head loss, m
K	pressure loss coefficient, $-$
L	length, m
N	number of channels, $-$
$\vec{N}$	unit normal vector, $-$
$NRMSE$	normalized root-mean-squared error, $-$
P	local pressure, Pa
Q	cumulative flow rate, m^3/s
q	flow rate, m^3/s
Re	Reynolds number , $-$
v	fluid local velocity, m/s
z	height, m

Greeks

α	flow distribution factor, $-$
ΔP	pressure drop, Pa
Δp	frictional pressure loss, Pa
ϵ	convergence error, $-$
ν	kinematic viscosity, m^2/s
ρ	fluid density, $\frac{kg}{m^3}$

Superscript

i	channel number

Subscripts

adj	adjusted
e	between two channels
exp	experiment
F	feed
f	friction
h	hydraulic
in	inlet
L	loss
M	mayor
m	minor
mod	model
new	new
out	outlet
ref	reference
T	tee junction
$Txin$	tee junction at the entrance of the channel
$Txout$	tee junction at the exit of the channel
$Tyin$	diverging-flow tee junction for the inlet manifold
$Tyout$	converging-flow tee junction for the outlet manifold
x	channel
y	manifold

Thermosiphon water systems are typically less expensive than active pump-driven systems and there is a growing interest to use PV/T collectors in thermosiphon water systems. Also, pressure drop over a solar collector gains importance since pressure drop is known to be an important factor for thermosiphon systems efficacy (Kalogirou, 2013). On the other side, flat-plate solar collectors are the usual type of collector for hybrid PV/T systems technology using water as coolant (Kalogirou and Tripanagnostopoulos, 2006). Accordingly, this paper presents a study made by DualSun on pressure drop in parallel flow flat-plate collectors in order to adapt the DualSun module, an innovative photovoltaic-thermal (PV/T) collector (Brottier et al. 2016), to be used in thermosiphon water systems. Fig. 1 shows a thermosiphon water system testbed where a DualSun module was installed in Marseille, France.

In this paper, first, a numerical model of a parallel flow collector is presented. Then, several fluid dynamic concepts are reviewed to calculate pressure drop over both the collector's manifold and the collector's channel. Next, an algorithm is used to calculate pressure distribution and pressure drop over the collector. Finally, the results of pressure drop measures over three flat-plate solar collectors with different manifold dimensions are presented and compared with the model results.

2. Mathematical Model

2.1 Variables and Flow distribution.

Parallel flow heat exchangers, or solar collectors, consist of an inlet and outlet manifold joined by a series of parallel channels where both inlet and outlet fluid flow are in the same direction, as shown in Fig. 2.

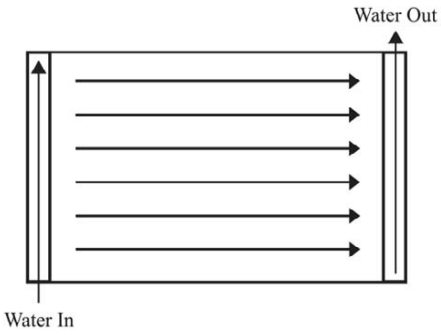

Fig. 2: Parallel flow collector diagram.

Several papers have analyzed the pressure drop over compact heat exchangers (Camilleri et al. 2015) and gas manifolds of a fuel-cell stack (Koh et al. 2003). In this paper an N-channel collector will be considered, and the channels will be numbered from the highest (1^{st}) to the lowest (N^{th}) position, where the input edge of the inlet manifold is in front of the N^{th} channel, and the output edge of the output manifold is in front of the 1^{st} channel, as shown in Fig. 3. Here $P_{in}^{(i)}$ denotes the pressure at the entrance of the i^{th} channel, $P_{out}^{(i)}$ denotes the pressure at the exit of the i^{th} channel and q_x^i is the water flow rate through the same channel. With this expression, pressure drop over each channel (i) is expressed by $\Delta P_x^{(i)}$, as shown in eq. 1.

Local pressure drop over the i^{th} inlet manifold section is expressed by eq. 2, and by eq. 3 for the case of the i^{th} outlet manifold section. Here, a manifold section (i) is defined from the entrance of the $(i-1)^{th}$ channel until the entrance of the i^{th} channel for inlet manifolds ('in' subscript and '(i)' superscript), and from the exit of the $(i-1)^{th}$ channel until the exit of the i^{th} channel for an outlet manifold section ('out' subscript and '(i)' superscript)

$$\Delta P_x^{(i)} = P_{in}^{(i)} - P_{out}^{(i)}, \quad (i = 1, \dots, N) \qquad \textit{(eq. 1)}$$

$$\Delta P_{in}^{(i)} = P_{in}^{(i)} - P_{in}^{(i-1)}, \quad (i = 2, \dots, N) \qquad \textit{(eq. 2)}$$

$$\Delta P_{out}^{(i)} = P_{out}^{(i)} - P_{out}^{(i-1)}, \quad (i = 2, \dots, N) \qquad \textit{(eq. 3)}$$

Then, cumulative flow rates $Q_{in}^{(i)}$ and $Q_{out}^{(i)}$ are defined as follows, where Q_F is the total inlet feed flow rate.

$$Q_{in}^{(i)} = \sum_{j=1}^{i} q_x^j = Q_{in}^{(i-1)} + q_x^i, \quad (i = 1, \dots, N) \qquad \textit{(eq.4)}$$

$$Q_{out}^{(i)} = \sum_{j=1}^{N} q_x^j = Q_{out}^{(i+1)} + q_x^i, \quad (i = 1, \dots, N) \qquad \textit{(eq. 5)}$$

$$Q_{in}^{(N)} = Q_F \qquad \textit{(eq. 6)}$$

2.2. Pressure Drop and Pressure Loss

In fluid mechanics, *pressure drop* is defined as the difference in pressure between two points of a fluid carrying network and which is due to the dissipation of mechanical energy into heat. Bernoulli's principle in fluid dynamics states that if there is conservation of energy, the following expression remains constant at any cross-sectional area *A* of a flowing fluid:

$$\int_A \left(\frac{P}{\rho} + \frac{v^2}{2} + gz\right) \rho \vec{v}.\vec{N}.\, dA \qquad \textit{(eq. 7)}$$

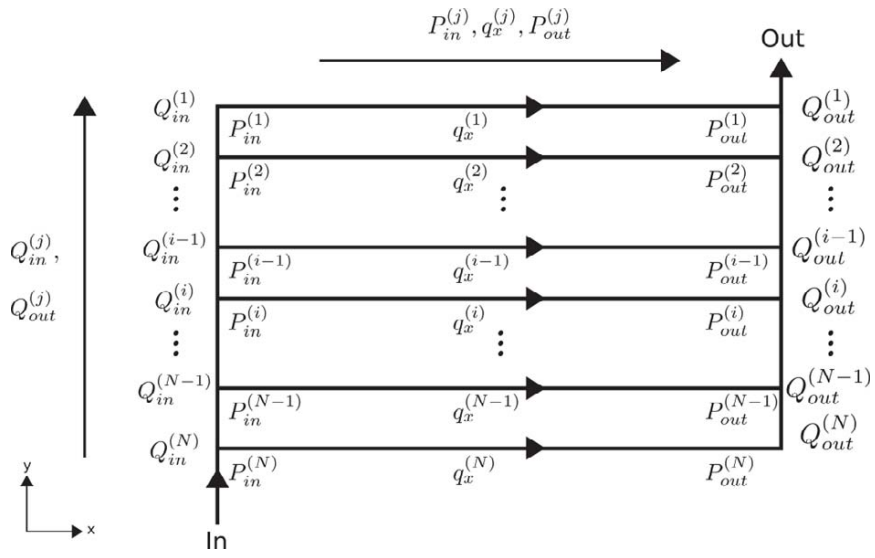

Fig. 3: Pressure and flow variables in the collector

Where P is pressure, ρ is the fluid density, v is the fluid local velocity, g is the acceleration due to gravity and z is the fluid height. Then, $\frac{P}{\rho}$ represents the flow work per unit mass, $\frac{v^2}{2}$ represents the kinetic energy per unit mass and gz represents the potential energy per unit mass. Some authors prefer to express eq. 7 in terms of energy per unit weight dividing it by the acceleration due to gravity. Considering the fluid pressure, fluid velocity and fluid height values as their mean values, along with assumed energy dissipation, the expression is no longer constant, and eq. 7 could be written in terms of energy per unit weight as:

$$\frac{\overline{P}_1}{\rho g} + \frac{\overline{\overline{v}_1^2}}{2g} + \overline{z}_1 = \frac{\overline{P}_2}{\rho g} + \frac{\overline{v}_2^2}{2g} + \overline{z}_2 + H_f \qquad \textit{(eq. 8)}$$

Here H_f represents the frictional work done per unit weight of a fluid element while moving from a point 1 to another point 2. H_f is called *head loss* and has a dimension of height. For simplicity, *frictional pressure loss* will be referred to as Δp_L , defined as:

$$\Delta p_L = \rho g H_f \qquad \textit{(eq. 9)}$$

Then, from eq. 2 we can calculate the *pressure drop*, defined as the pressure difference (in mean value) of a fluid while moving from a point 1 to a point 2, expressed then as the following:

$$\Delta P = \overline{P}_1 - \overline{P}_2 = \rho \frac{\overline{v}_2^2 - \overline{v}_1^2}{2} + \rho g(\overline{z}_2 - \overline{z}_1) + \Delta p_L \qquad \textit{(eq. 10)}$$

Pressure loss depends on any type of head loss H_f as described in eq. 9. Head losses, on their side, are divided in two main categories: *major head losses* (H_M) due to viscosity and wall friction along a pipe, and *minor head losses* (H_m) due to changes in the cross-section of the flow such as junction and bends. Major head losses can be calculated using the Darcy-Weisbach equation as shown in eq. 11, where f is the *Darcy friction factor*, L is the length of the pipe and D_h is the hydraulic diameter of the pipe. Minor head losses, for their part, depend on the *local loss coefficient K,* as shown in eq. 12.

$$H_M = f\frac{Lv^2}{2gD_h} \qquad \textit{(eq. 11)}$$

$$H_m = K\frac{v^2}{2g} \qquad \textit{(eq. 12)}$$

Having explained each type of head loss, the *total head loss* H_f is defined as the sum of major head losses and minor head losses, and total pressure loss becomes:

$$\Delta p_L = \rho g(H_M + H_m) = f\frac{\rho L v^2}{2D_h} + K\frac{\rho v^2}{2} \qquad \textit{(eq.13)}$$

Combining eq. 10 and eq. 13, pressure drop can then be written as:

$$\Delta P = \rho\frac{\bar{v}_2^2 \cdot \bar{v}_1^2}{2} + \rho g(\bar{z}_2 - \bar{z}_1) + f\frac{\rho L v^2}{2D_h} + K\frac{\rho v^2}{2} \qquad \textit{(eq. 14)}$$

2.3. Darcy friction factor f and the loss coefficient K

The Darcy friction factor f and the loss coefficient K of the last expression (eq. 14) have been widely studied (Hager, 2010; Koch, 2000). The Darcy friction factor is a function on the dimensionless Reynolds number Re and depends on whether the flow is laminar or turbulent. The Reynolds number is defined as shown in the following equation, where ν is the kinematic viscosity of the fluid:

$$Re = \frac{vD_h}{\nu} \qquad \textit{(eq. 15)}$$

Here, an approximate way to calculate the Darcy friction factor is presented. For laminar flow ($Re < 2300$), the Darcy friction factor can be calculated as eq. 16; and for turbulent flow ($Re > 2300$), the Blasius equation is used as shown in eq.17

$$f = \frac{64}{Re}, \qquad Re < 2300 \qquad \textit{(eq. 16)}$$

$$f = 0.3164\, Re^{-0.25}, \qquad Re > 2300 \qquad \textit{(eq. 17)}$$

Koch (2000) has made a survey of available data of the pressure loss coefficient K for elbows and tees of pipework. The survey shows that in tee joints the K factor depends considerably on the tee configuration (converging flow, diverging flow) and which flow is being considered (from the branch, along the straight, etc.). The velocity used to calculate the minor head loss shown in eq. 12 is the velocity of the combined flow. For further information, see the articles listed in the Reference section.

2.4 The solar collector and pressure drop

In order to calculate pressure drop over the solar collector, an expression will firstly be given to calculate the pressure drop in each channel and in each manifold, based on the variables defined before.

Pressure drop over each channel strongly depends on the channel geometry and the presence of tee junctions or bends as explained in the previous section. If we consider the *channel flow* as the flow starting from the inlet manifold until the outlet manifold, both the tee junction diverging the flow from the inlet manifold and the tee junction converging the flow at the outlet manifold should be considered as minor head losses, each one with its own loss coefficient K. In the following, the subscript *Txin* will be used to describe the effects of the tee junction at the entrance of the channel, while the subscript *Txout* will be used to describe the effects of the tee junction at the exit of the channel. As there is no change in the flow, the fluid velocity through the channel (v_x) remains constant. Using the pressure drop expression introduced in eq. 14, and assuming that there is no change in height, eq. 1 becomes:

$$\Delta P_x^{(i)} = \Delta p_{L_{Tin}}^{(i)} + \Delta p_{L_x}^{(i)} + \Delta p_{L_{Tout}}^{(i)} = \frac{\rho}{2}\left(f_x\frac{L_x {v_x^{(i)}}^2}{D_{h_x}} + K_{Txin}^{(i)} {v_{y_{in}}^{(i)}}^2 + K_{Txout}^{(i)} {v_{y_{out}}^{(i)}}^2\right) \qquad \textit{(eq.18)}$$

Here, the fluid velocity through both intlet ($v_{y_{in}}$) and outlet ($v_{y_{out}}$) manifold are used to calculate the minor head losses since for tee junctions the velocity of the combined flow should be considered. However, the same superscript is used to simplify the solution algorithm. For the first and the last channel, the loss coefficient corresponding to elbows should be considered (Koch, 2000). Velocities are defined as the flow rate divided by the cross section flow area.

For the case of manifolds, the fluid flow rate decreases from the feeding position to the other end, with an inverse effect for the outlet manifold as the flow from each channel is sequentially added to the main flow.

Thus, the fluid velocity change should be considered. Additionally, only one tee junction will be taken into account. For simplification in the following, the subscript *Tyin* will be used to describe the effect of the diverging-flow tee junction (with flow going to the branch) for the inlet manifold, while the subscript *Tyout* will be used to describe the effect of the converging-flow tee junction (with flow coming from the branch) for the outlet manifold. Using the pressure drop expression introduced in eq. 14, and assuming that there is no change in height, eq. 5 and eq. 6 becomes eq. 19 for the local pressure drop in an inlet manifold section, and eq. 20 for the local pressure drop in an outlet manifold section, where L_e is the distance between two channels.

$$\Delta P_{in}^{(i)} = \rho \frac{\bar{v}_{y_{in}}^{(i-1)^2} - \bar{v}_{y_{in}}^{(i)^2}}{2} + \Delta p_{L_{Tyin}}^{(i)} + \Delta p_{L_y}^{(i)} = \frac{\rho}{2}\left(v_{y_{in}}^{(i-1)^2} - v_{y_{in}}^{(i)^2} + f_y \frac{L_e v_{y_{in}}^{(i)\ 2}}{D_{h_y}} + K_{Tyin}^{(i)} v_{y_{in}}^{(i)\ 2} \right) \quad \textit{(eq. 19)}$$

$$\Delta P_{out}^{(i)} = \rho \frac{\bar{v}_{y_{out}}^{(i-1)^2} - \bar{v}_{y_{out}}^{(i)^2}}{2} + \Delta p_{L_{Tyin}}^{(i)} + \Delta p_{L_y}^{(i)} = \frac{\rho}{2}\left(v_{y_{out}}^{(i-1)^2} - v_{y_{out}}^{(i)^2} + f_y \frac{L_e v_{y_{out}}^{(i)\ 2}}{D_{h_y}} + K_{Tyout}^{(i)} v_{y_{out}}^{(i)\ 2} \right) \textit{(eq. 20)}$$

2.5 Solution algorithm

In the following, a modified algorithm first introduced by Koh et al (2002) is presented to calculate pressure distribution and pressure drop over the collector.

Starting from an equally-divided channel flow rate ($q_x^{(i)} = Q_F/N$), the cumulative local flow rates in manifolds $Q_{in}^{(i)}$and $Q_{out}^{(i)}$ are obtained from eqs. 4 and 5. To continue, a reference local pressure in the outlet manifold $P_{out_{ref}}^{(1)} = P_{ref} = 0$ is defined, defining also a channel pressure drop reference $\Delta P_x^{(1)}{}_{ref}$ and a local pressure in the inlet manifold $P_{in}^{(1)}{}_{ref}$ using eqs.1 and 2. Then, sequentially, the pressure drop in outlet manifold $\Delta P_{out}^{(i)}$ and local pressure $P_{out}^{(i)}$ are calculated. $\Delta P_{out}^{(i)}$ is calculated using eq.20, while $P_{out}^{(i)}$ is calculated using eq. 3. The next step is to calculate sequentially the local pressure in the inlet manifold $P_{in}^{(i)}$ using eqs. 19 and 2.

In the following, a *flow distribution factor* $\alpha^{(i)}$ shown in eq. 22 is defined to be used as a redundant parameter in order to sequentially adjust channels flow rates in each iteration step until convergence is reached.

$$\alpha^{(i)} = \frac{P_{in}^{(i)} - P_{out}^{(i)}}{\Delta P_x^{(1)}} \quad \textit{(eq. 21)}$$

The adjustment correlation is developed from the definition of the flow distribution factor:

$$\sum_{i=1}^{N} \alpha^{(i)} = \frac{\sum_{i=1}^{N}\left[P_{in}^{(i)} - P_{out}^{(i)}\right]}{\Delta P_x^{(1)}} \quad \textit{(eq. 22)}$$

From this expression, a new value of the pressure drop over the first channel is obtained to adjust all local pressure and pressure drop values systematically as shown in the following expression:

$$\Delta P_x^{(1)} = \frac{\sum_{i=1}^{N}\left[P_{in}^{(i)} - P_{out}^{(i)}\right]}{\sum_{i=1}^{N} \alpha^{(i)}} \quad \textit{(eq. 23)}$$

By substituting the pressure drop terms, $P_{in}^{(i)} - P_{out}^{(i)}$ in eq. 23 by the equation for pressure drop over channels $\Delta P_x^{(i)}$ (eq.18), the expression becomes:

$$\Delta P_x^{(1)} = \frac{\sum_{i=1}^{N}\left[P_{in}^{(i)} - P_{out}^{(i)}\right]}{\sum_{i=1}^{N} \alpha^{(i)}} = \frac{\sum_{i=1}^{N} \Delta P_x^{(i)}}{\sum_{i=1}^{N} \alpha^{(i)}} = \frac{\sum_{i=1}^{N} \frac{\rho}{2}\left(f_x \frac{L_x v_x^{(i)^2}}{D_{h_x}} + K_{Txin}^{(i)} v_{y_{in}}^{(i)\ 2} + K_{Txout}^{(i)} v_{y_{out}}^{(i)\ 2} \right)}{\sum_{i=1}^{N} \alpha^{(i)}} \quad \textit{(eq. 24)}$$

Here, it is important not to replace the flow distribution factor by its formula, but to use the already calculated values. Once all local pressure and pressure drop values are adjusted, the flow distribution factor should be adjusted as well. Finally, new channel flow rates are then calculated from the adjusted inlet manifold pressure values using the flow rate definition (eq. 25) and eq. 18, as shown in eq. 25 and 26, whereA_x is the channel cross-sectional area.

$$q_{x\ new}^{(i)} = A_x v_{x\ new}^{(i)} \qquad \textit{(eq. 25)}$$

$$q_{x\ new}^{(i)} = A_x \sqrt{\frac{D_h}{f L_x}\left(\frac{2}{\rho}\left(P_{in\ adj}^{(i)} - P_{out}^{(i)}\right) - K_{Txin}^{(i)} v_{y_{in}}^{(i)\ 2} - K_{Txout}^{(i)} v_{y_{out}}^{(i)\ 2}\right)} \qquad \textit{(eq. 26)}$$

Note that the outlet manifold pressure is not adjusted because the exit pressure is known and is equivalent to the outlet reference pressure $(P_{out_{ref}}^{(1)} = P_{ref} = 0)$. Once new channels flow rates are determined, they are compared with the initial or the previously calculated channel flow rates. The calculation continues with a new set of channel flow rates until the $q_x^{(i)}$ values are close to the old values within an error limit. The entire solution algorithm is summarized in Appendix A.

3. Experimental

Three flat-plate solar collectors as shown in Figs.4 and 5 with different manifold dimensions where used to measure pressure drop, using water columns to measure pressure and an electronic flow meter to measure the water flow rate in the collector inlet. The width and depth of the manifolds where respectively: 0.035x0.035m (collector N°1) 0.02x0.007m (collector N°2) and 0.045x0.045m (collector N°3). All other dimensions where equal as shown in Table 1.

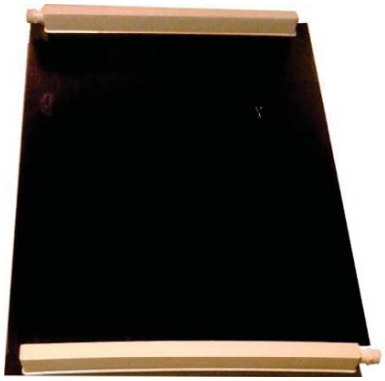

Fig. 4: Parallel flat-plate solar collector with rectangular manifold.

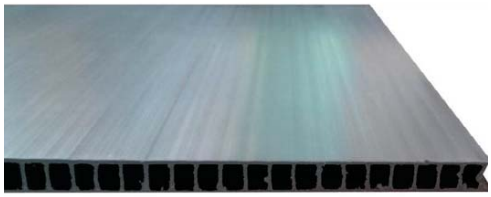

Fig. 5: Cross-sectional view of the collector channels.

Tab. 1: Manifold Dimensions

	Manifold Width [m]	Manifold Depth [m]	Manifold Large [m]	Channel Large[m]	Channel Width [m]	Channel Depth [m]	Number of Channels
Collector N°1	0.035	0.035	0.954	1.4	0.004	0.0044	165
Collector N°2	0.02	0.007	0.954	1.4	0.004	0.0044	165
Collector N°3	0.045	0.045	0.954	1.4	0.004	0.0044	165

4. Results

The three collector pressure drop measurements and simulations are compared in Fig. 6-9. The model is compared with the experiment values using the normalized root-mean-squared error (NRMSE) as defined in eq. 25. Finally, a pressure drop prediction is made for four solar collectors with different squared manifold dimensions (Fig. 4) in order to show the influence of the manifold size on the solar collector pressure drop.

$$NRMSE = \sqrt{\frac{1}{n}\sum_j^n (\Delta P_{exp} - \Delta P_{mod})^2} \,/\, (\Delta P_{mod}^{max} - \Delta P_{mod}^{min})$$

(eq. 27)

It can be seen that at some point (a=0.045m), pressure drop becomes less sensitive to increasing manifold width or depth in 0.005m when comparing to a smaller manifold (a=0.020m). This is probably because manifold size becomes proportionally less important and the analysis must be extended to the channels dimensions.

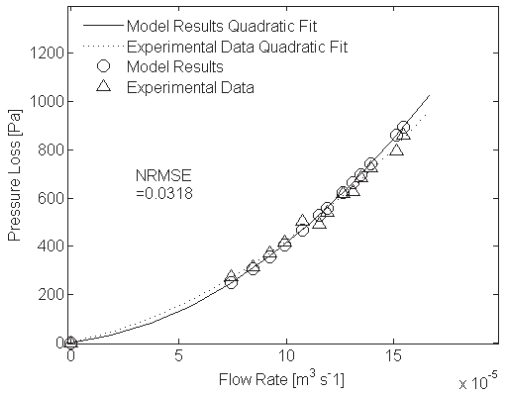

Fig. 6: Comparison of the predicted and measured pressure drop for the collector N°1

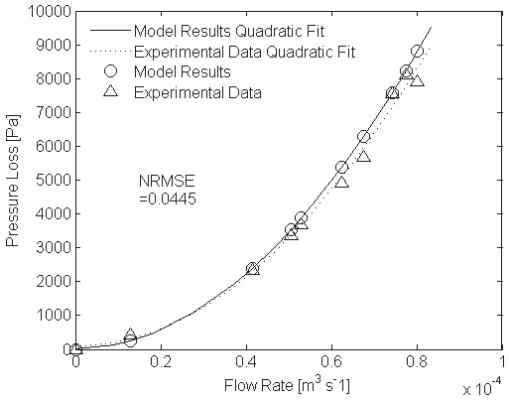

Fig. 7: Comparison of the predicted and measured pressure drop for the collector N°2

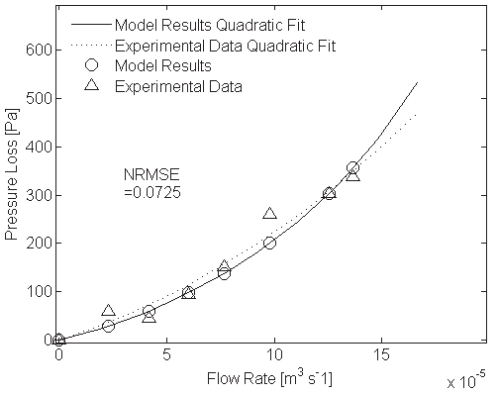

Fig. 8: Comparison of the predicted and measured pressure drop for the collector N°3

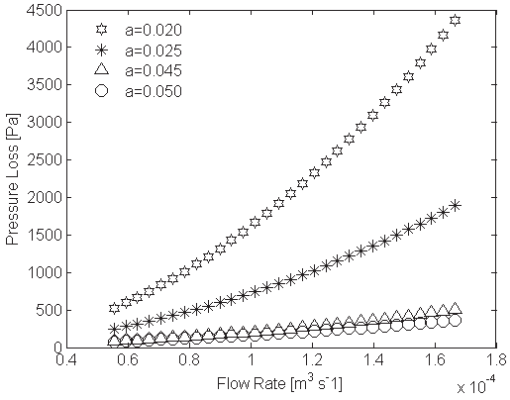

Fig. 9: Pressure drop predictions for different squared manifold dimensions (width=depth=a).

5. Conclusions

This paper presents a reliable numerical model and solution algorithm to calculate the pressure drop over parallel flow flat-plate solar collectors. The model gives the possibility to simulate pressure drop over exchangers at an early design stage and investigate the effects of geometric dimensions such as manifold or channel size. For the case of flat-plate PV/T solar collectors to be used in thermosiphon water systems, this model can be used to investigate trade-offs between fabrication choices and the thermosiphon performance.

Three flat-plate solar collectors with different manifold dimensions were used as a test case in which the model was validated within 3-8% in terms of normalized root-mean-square deviation. Also, the influence of the manifold size on the solar collector pressure drop was analyzed. It is shown that for smaller manifold size, the incremental pressure drop is higher than for larger manifolds. A channels size sensibility was not studied and should be take into account in further studies.

6. References

Brottier L., Naudin S., Veeser V., Terrom G., Bennacer R., 2016. Field test results of an innovative PV/T collector for solar domestic hot water. Energy Procedia. 91, 276-283.

Camilleri R., Howey D.A., McCulloch M.D., 2015. Predicting the flow distribution in compact parallel flow heat Exchangers. Applied Thermal Engineering. 90, 551-558, with permission from Elsevier.

Hager W.H., 2010. Losses in Flow, in: Wastewater Hydraulics, second ed., Springer-Verlag, Berlin-Heidelberg, pp. 17-54

Kalogirou S., Tripanagnostopoulos Y. 2006. Hybrid PV/T solar systems for domestic hot water and electricity production. Energy Converssion and Management. 47, 3368–3382.

Kalogirou S., 2013. Thermosiphon solar water-heating systems, in: Solar Energy Engineering, second ed., Elsevier/Academic Press, Amsterdam-London, pp 606-618.

Koch P., 2000. A survey of available data for pressure loss coefficients, z for elbows and tees of pipework. Building Services Engineering Research & Technology. 21, 153-160.

Koh J.H., Seo H.K., Lee C.G., Yoo Y.S., Lim H.C., 2003. Pressure and flow distribution in internal gas manifolds of a fuel cell stack. Journa of Power Sources. 115, 54-65.

Wysocki J. J., Rappaport P. 1960. Effect of temperature on photovoltaic solar energy conversion. Journal of Applied Physics. 31, 571–578.

Appendix: **Algorithm to calculate pressure drop over flat-plate solar collectors**

Step 1: Initial guess of channel flow rates and a reference inlet pressure drop.

$$q_x^{(i)} = \frac{Q_F}{N}, \quad (i = 1 \text{ to } N) \qquad \textit{(eq.A.1)}$$

$$v_x^{(i)} = \frac{q_x^{(i)}}{A_x}, \quad (i = 1 \text{ to } N) \qquad \textit{(eq.A.2)}$$

$$\Delta P_x^{(1)}{}_{ref} = \frac{\rho}{2}\left(f_x \frac{L_x v_x^{(i)\,2}}{D_{h_x}} + K_{Txin}^{(i)} v_{y_{in}}^{(i)\,2} + K_{Txout}^{(i)} v_{y_{out}}^{(i)\,2} \right) \qquad \textit{(eq.A.3)}$$

Step 2: Calculate flow rates and linear velocity in manifolds and Reynolds numbers.

$$Q_{in}^{(i)} = Q_{in}^{(i-1)} + q_x^i, \quad (i = 1, \ldots, N) \qquad \textit{(eq.A.4)}$$

$$Q_{out}^{(i)} = Q_{out}^{(i+1)} + q_x^i, \quad (i = 1, \ldots, N) \qquad \textit{(eq.A.5)}$$

$$v_{y_{in}}^{(i)}, v_{y_{out}}^{(i)}, Re_{y_{out}}^{(i)}, Re_{y_{out}}^{(i)}, Re_x^{(i)}$$

Step 3: Calculate outlet manifold pressure.

$$P_{out_{ref}}^{(1)} = P_{ref} = 0 \qquad \textit{(eq.A.6)}$$

- *Loop 3.1: For i= 2 to N:*

$$\Delta P_{out}^{(i)} = \frac{\rho}{2}\left(v_{y_{out}}^{(i-1)^2} - v_{y_{out}}^{(i)^2} + f_y \frac{L_e v_{y_{out}}^{(i)\,2}}{D_{h_y}} + K_{Tyout}^{(i)} v_{y_{out}}^{(i)\,2} \right) \qquad \textit{(eq.A.7)}$$

$$P_{out}^{(i)} = \Delta P_{out}^{(i)} + P_{out}^{(i-1)} \qquad \textit{(eq. A.8)}$$

Step 4: Calculate inlet manifold pressure.

$$P_{in\ ref}^{(1)} = \Delta P_x^{(1)}{}_{ref} + P_{out_{ref}}^{(1)} \qquad \textit{(eq.A.9)}$$

- *Loop 4.1: For i= 2 to N:*

$$\Delta P_{in}^{(i)} = \frac{\rho}{2}\left(v_{y_{in}}^{(i-1)^2} - v_{y_{in}}^{(i)^2} + f_y \frac{L_e v_{y_{in}}^{(i)\,2}}{D_{h_y}} + K_{Tyin}^{(i)} v_{y_{in}}^{(i)\,2} \right) \qquad \textit{(eq.A.10)}$$

$$P_{in}^{(i)} = P_{in}^{(i-1)} + \Delta P_{in}^{(i)}, \qquad \textit{(eq. A.11)}$$

Step 5: Calculate flow distribution factors.

$$\alpha^{(i)} = \frac{P_{in}^{(i)} - P_{out}^{(i)}}{\Delta P_x^{(1)}}, \quad (i = 1, \ldots, N) \qquad \textit{(eq. A.12)}$$

Step 6: Calculate a new value of the pressure drop over the first channel

$$\Delta P_x^{(1)}{}_{new} = \frac{\sum_{i=1}^{N} \frac{\rho}{2}\left(f_x \frac{L_x v_x^{(i)\,2}}{D_{h_x}} + K_{Txin}^{(i)} v_{y_{in}}^{(i)\,2} + K_{Txout}^{(i)} v_{y_{out}}^{(i)\,2} \right)}{\sum_{i=1}^{N} \alpha^{(i)}} \qquad \textit{(eq. A.13)}$$

Step 7: Adjust local inlet manifold pressure from new pressure drop over the first channel

$$P_{in\ adj}^{(1)} = \Delta P_x^{(1)}{}_{new} + \Delta P_{out}^{(1)} \qquad \textit{(eq. A.14)}$$

$$P_{in\ adj}^{(i)} = P_{in\ adj}^{(i-1)} + \Delta P_{in}^{(i)}, \quad (i = 2, \ldots, N) \qquad \textit{(eq. A.15)}$$

Step 8: Adjust flow distribution factors from new pressure drop over the first channel.

$$\alpha^{(i)}{}_{adj} = \frac{P^{(i)}_{in\,adj} - P^{(i)}_{out}}{\Delta P^{(1)}_{x\,new}}, \quad (i = 1, \ldots, N) \qquad \textit{(eq. A.16)}$$

Step 9: Calculate new set of channel flow rates form adjusted inlet manifold pressure.

$$q^{(i)}_{x\,new} = A_x \sqrt{\frac{D_h}{fL_x}\left(\frac{2}{\rho}\left(P^{(i)}_{in\,adj} - P^{(i)}_{out}\right) - K^{(i)}_{Txin} v^{(i)\,2}_{y_{in}} - K^{(i)}_{Txout} v^{(i)\,2}_{y_{out}}\right)}, \quad (i = 1, \ldots, N) \qquad \textit{(eq. A.17)}$$

Step 10: Check convergence.

$$ERR = \sum_{i=1}^{N} \left[\frac{q^{(i)}_{x\,new} - q^{(i)}_{x}}{q^{(i)}_{x}}\right]^2 \qquad \textit{(eq. A.18)}$$

In $ERR > \epsilon$*, update* $\Delta P_x^{(1)}$ *and* $q_x^{(i)}$*, and go to Step 2. If* $ERR < \epsilon$*, stop.*